Separation Science and Technology
Publication details, including instructions for authors and subscription information:
http://www.informaworld.com/smpp/title~content=t713708471

Effect of Cyclic Changes in Temperature and Pressure on Permeation Properties of Composite Polyamide Seawater Reverse Osmosis Membranes

M. F. A. Goosen[a]; S. Sablani[b]; M. Dal Cin[c]; M. Wilf
[a] Office of Research, Alfaisal University, Riyadh, Saudi Arabia [b] Department of Biological Systems Engineering, Washington State University, Pullman, WA, USA [c] ICPET, National Research Council Canada, Ottawa, Ontario, Canada

Online publication date: 20 December 2010

To cite this Article Goosen, M. F. A. , Sablani, S. , Cin, M. Dal and Wilf, M.(2011) 'Effect of Cyclic Changes in Temperature and Pressure on Permeation Properties of Composite Polyamide Seawater Reverse Osmosis Membranes', Separation Science and Technology, 46: 1, 14 — 26
To link to this Article: DOI: 10.1080/01496395.2010.502552
URL: http://dx.doi.org/10.1080/01496395.2010.502552

Separation Science and Technology, 46: 14–26, 2011

ISSN: 0149-6395 print/1520-5754 online
DOI: 10.1080/01496395.2010.502552

Taylor & Francis
Taylor & Francis Group

Effect of Cyclic Changes in Temperature and Pressure on Permeation Properties of Composite Polyamide Seawater Reverse Osmosis Membranes

M. F. A. Goosen,[1] S. Sablani,[2] M. Dal Cin,[3] and M. Wilf[4]
[1]*Office of Research, Alfaisal University, Riyadh, Saudi Arabia*
[2]*Department of Biological Systems Engineering, Washington State University, Pullman, WA, USA*
[3]*ICPET, National Research Council Canada, Ottawa, Ontario, Canada*
[4]*San Diego, CA, USA*

The effects of cyclic changes in feed water temperature and pressure on permeate flux, solute rejection, and compaction in spiral wound composite polyamide seawater reverse osmosis membranes were examined with pure water and 4% NaCl solutions. A membrane permeability hysteresis or memory effect due to the up and down temperature and pressure sequences was only seen with the saline water studies. However, the observed changes appeared to be reversible and were consistent with the Spiegler-Kedem/ Film Theory and the Kimura-Sourirajan Analysis/ Film Theory models. The overall results suggest that the net effect on permeance and solute rejection is the consequence of several interactions with feed/operating temperatures affecting membrane porosity and water/solute cluster size, and transmembrane pressure influencing membrane compaction.

Keywords compaction; cyclic changes in temperature and pressure; Kimura-Sourirajan analysis/film theory model; membrane permeability hysteresis; polyamide RO membranes; Spiegler-Kedem/film theory model

INTRODUCTION

Membrane separation processes are widely used in water desalination, biochemical processing, industrial wastewater treatment, food and beverage production, and pharmaceutical applications (1–11). Composite polyamide membranes, for example, have been modified with carbon nanotubes as well as being synthesized on an ultraporous substrate for applications in pervaporation (12–13). Membrane lifetime and permeate fluxes are primarily affected by the phenomena of concentration polarization (i.e., solute build-up) and fouling (e.g., microbial adhesion, gel layer formation, and solute adhesion) at the membrane surface (14–21). Koltuniewicz and Noworyta (22) assessed the phenomena responsible for limiting the permeate flux during cyclic operation (i.e., permeation followed by cleaning). Manttarii et al. (23) investigated the effect of temperature and membrane pre-treatment by pressure on the filtration properties of nanofiltration membranes. While the effect of membrane fouling on flux has received extensive attention, the effect of feed temperature on the flux is one area where more research is needed (24,25).

Reverse Osmosis (RO) desalination equipment in hot and arid regions, such as the Arabian Gulf, must operate under very high average daytime temperatures. This contrasts sharply with temperatures in temperate regions, such as the US, Europe, or Japan, which produce most commercial reverse osmosis membranes. Operating conditions in these countries are at moderate temperatures. Air temperatures over 50°C in desalination plants, a condition in many Arabian Gulf countries during the summer, will result in high feed water temperatures and may lead to permanent changes within a membrane, as has been observed by Mantarrii et al. (23) for nanofiltration of industrial streams at elevated temperatures. Goosen et al. (6) showed that composite polyamide RO membranes can be very sensitive to changes in the feed water temperature. There was up to a 100% difference in the permeate flux between feed temperatures of 30°C and 40°C.

Combined high temperature and high pressure operation may cause permanent damage (i.e., compaction) to RO/UF(ultrafiltration)/NF(nanofiltration) membranes (24–28). This could take the form of changes in the structure and morphology of the polymer matrix comprising the membrane barrier layer. Sizes of pores in the active layer of polymeric NF membranes can be expected to depend on the operating temperature and pressure (26,29,30). Pore size distributions can be derived to interpret changes in membrane selectivity towards solutes with temperature and Stokes radius. Vazquez and Benavente (28) obtained a decrease in the hydraulic

Received 22 February 2010; accepted 16 June 2010.
Address correspondence to M. F. A. Goosen, Office of Research, Alfaisal University, P.O. Box 50927, Riyadh 11533, KSA. Tel.: +966 53 294 1468. E-mail: mgoosen@alfaisal.edu

resistance of regenerated cellulose membranes as a result of annealing at 60°C. This indicated a more open structure in the polymer matrix. Chemical degradation was confirmed with X-ray photoelectromicroscopy. In addition to possible membrane compaction/morphological effects, leakages may occur in spiral-wound modules due to pinholes, at glue lines and at the connections between two elements (e.g., at the O-rings) (27).

Sharma et al. (26), working with a commercially available composite polyamide membrane (i.e., DL by Osmonics), showed that the temperature correction factor for the flux (normalized to 25°C), valid in the temperature range $5 \leq T \leq 41$°C, took the form:

$$\frac{J_{v,T}}{J_{v,25^\circ C}} = \exp\left[2918\left(\frac{1}{298} - \frac{1}{273+T}\right)\right] \quad (1)$$

where $J_{v,T}$ is the volume flux at any temperature T (*in* °C) and $J_{v,25°C}$ is the corresponding flux at 25°C. The constant, 2918 units K (kelvin), in Eq. (1) is specific for the polymer in the membrane barrier and has been termed the activation energy for flow comprising viscous and other contributions. Membrane manufacturers employ similar equations for temperature correction factors of RO membranes (26). Pore size studies have also been performed with amorphous silica materials (31).

Changes in membrane properties at different pressures and temperatures can be identified by studying changes in the permeance (i.e., pressure normalized flux or flux/transmembrane pressure). Temperature changes will affect the viscosity of the water, which will influence the permeation of water through the membrane. The permeance, L, (i.e., flux/pressure) may be corrected for temperature using (32):

$$L_{T2} = (\mu_{T1}/\mu_{T2})L_{T1} \quad (2)$$

where μ is the viscosity of the water at temperature T. Equation 2 can be used to remove viscosity effects from the flux measurements. If these effects are the only factors leading to an increase in flux then the corrected permeance should not be a function of temperature. The viscosity of water from 20 to 100°C in centiPoise at temperature T_1 may be determined by (32) referenced to a viscosity of 1.002 cP at 20°C:

$$\mu_{T1} = \exp_{10}\frac{1.3272\times(20-T_1) - 0.001053\times(T_1-20)^2}{(T_1+105)\times 1.002} \quad (3)$$

Changes in the permeance can indicate a change in the membrane itself or an inadequacy of the viscosity correction. The viscosity correction assumes that Newtonian flow still applies at sub nanometer pore dimensions.

Permeances, L, measured with NaCl solutions are corrected for the osmotic pressure of the feed at the wall and the permeate (26,32):

$$L = \frac{Jv}{\Delta P - (\Pi_{FW} - \Pi_P)} \quad (4)$$

where Π_{FW}, the osmotic pressure at the membrane wall, was determined from the y-intercept of J_v vs feed pressure plots and Π_P, the osmotic pressure of the permeate, was determined from conductivity measurements, $\triangle P$ refers to the transmembrane pressure.

The main objectives of our study were to assess the effects of cyclic changes in feed water temperature and pressure on the permeate flux, solute rejection, and compaction in the spiral wound composite polyamide seawater reverse osmosis membranes. The data was then used to assess whether flux/solute rejection changes were caused by reversible/irreversible physical changes in the membrane and/or to changes in the viscosity of the water. The experimental data was also modelled and membrane transport parameters were estimated.

EXPERIMENTAL

Equipment

Experiments were carried out using a pilot scale UF/RO unit (Armfield Ltd, UK) and a 1 m long pressure vessel module (Model 25 M 100AL, Hydranautics Inc., USA) containing a spiral wound membrane element (RO: SWC1-2540; Hydranautics Inc., USA). The RO membrane (SWC1-2540) was a composite polyamide with a 0.0508 cm spacer and a membrane area of 3.066 m^2. Nominal element performance, based on manufacturer specifications is: salt rejection 99.6% (32,000 ppm NaCl), maximum operating temperature 45°C, maximum applied pressure 1200 psig (i.e., 83 bar). The membranes were stored in a saline solution. The elements were rinsed with distilled water for 10 minutes at 20 bar prior to use.

Pressure readings were taken using analogue gauges attached to the pressure vessel. The pressure drop along the membrane length was found to increase from 0.1 to 0.3 bar as the pressure at the membrane inlet increased. The recirculation rate was kept constant at 9 L/min for the RO experiments (or 540 L/hr) when the pressure was increased.

Two types of feed water solutions were employed—distilled water and 4% (wt) NaCl for the RO experiments. All experiments were performed in triplicate.

Temperature and Pressure Effects on Pure Water Permeance

An initial study was performed with pure water to assess permeation properties in the absence of concentration

polarization. Flux measurements were taken at a range of temperatures and pressures to determine the effect of these on the flux of the permeate water. For each temperature, the feed pressure was varied between 20 to 50 bar at 10 bar intervals. The temperature was varied between 20 to 50°C in 10 degree steps. In some experiments the RO unit was run for 1–2 hours to assess the possibility of membrane compaction. Flux measurements were taken by collecting permeate water for two minutes and measuring its' volume. During a typical two minute period, for example, 4 L water would be collected. Assuming a maximum error of ± two seconds in the sampling time, this would result in an error of ±0.07 L in the volume of the collected permeate and ±2% in the flux readings.

The temperature of the feed water was varied using two sequences—up: 20°C, 30°C, 40°C, 50°C, and down: 50°C, 40°C, 30°C, and 20°C. At each temperature, the permeate flux measurements were taken at pressures of 20, 30, 40, and 50 bar. In some experiments the pressure changes were also run in an up and down sequence.

Two methods were used to heat the feed water. In the first, high temperatures were reached by running the system at 50 bar until the desired temperature was obtained. The pressure was then reduced to the value for that experiment, steady state was typically achieved in minutes, before the permeate rate was measured. With this method for heating the feedwater, there was some concern about the thermal equilibrium of the system. Therefore, in later experiments an electrical heating coil was employed.

The maximum temperature variation during an experiment was ±0.5°C. The viscosity corrected permeance was calculated using Eqs. (2) and (3).

Temperature and Pressure Effects on Permeance in Reverse Osmosis of 4% Saline Solution

In the studies with saline solutions, a nominal salt concentration of 4% (w/v) was employed which is roughly the same concentration as is found in seawater (i.e., 32,000 PPM). For these experiments, due to the high osmotic pressure of the saline water (i.e., 33.4 bar), only three pressures (on feed side) could be used, 40, 45, and 50 bar. The temperature of the feed was maintained using indirect external heating and cooling. For heating, an electric resistance coil was used while ice cold water was employed for cooling. The RO unit was run for 1–2 hours to allow for membrane compaction, if any. Then permeate samples were collected for 2–3 minutes. The salinity of the feed and the permeate was tested at room temperature (i.e., 25°C) using a conductivity meter.

The observed rejection was calculated using:

$$R_o = 1 - \frac{C_P}{C_{FC}} \tag{5}$$

where C_P and C_{FC} are the salt concentrations in the permeate and corrected feed respectively.

Weight% concentrations of aqueous NaCl solutions were correlated with conductivity, divided into two concentration ranges, and correlated using power law type expressions. The first covered concentrations from 0.0001 to 1 wt% and was used to convert measured conductivities to concentrations to calculate R_o for permeates from the RO data. The correlation, Eq. (6a), where S is in μS/cm:

$$C_{\mathrm{NaCl}} = 4.1014860 \times 10^{-5} \times \mathrm{S}^{1.0286182} \tag{6a}$$

uses the equivalent conductance values from the CRC Handbook of Chemistry and Physics (33). A comparison with two other sources showed very good agreement (data not shown). The second concentration range spanned 1 to 10 wt% NaCl and is based on data from the Cole-Palmer Handbook. It is correlated with the conductivity S, in mS/cm by:

$$C_{\mathrm{NaCl}} = 2.0136150 \times 10^{-5} \times \mathrm{S}^{1.104794} \tag{6b}$$

Equation (6b) is used to convert feed salinities to wt% concentrations.

The average of the feed concencentration at the inlet, C_{Fi}, and outlet, C_{Fo}, was used to account for the salt concentration recovered in the module, C_{FR}:

$$C_{FR} = \frac{1}{2}(C_{Fi} + C_{Fo}) \tag{7a}$$

Using a mass balance on the RO unit we can put C_{Fo} in terms of C_{Fi} and C_P:

$$C_{Fo} = \left(\frac{(C_{Fi}Q_F - C_PQ_P)}{(Q_F - Q_P)}\right) \tag{7b}$$

where C_{Fi} is the initial feed concentation in the tank, C_{Fo} is the outlet feed concentation in the tank, C_P is the salt concentration in permeate, and Q_F and Q_P are the retentate flow rates at the inlet and permeate outlet of the module respectively. Substituting Eq. (7b) into Eq. (7a) gives:

$$C_{FR} = \frac{1}{2}\left(C_{Fi} + \frac{(C_{Fi}Q_F - C_PQ_P)}{(Q_F - Q_P)}\right) \tag{7c}$$

An additional correction was applied to the concentration of the feed in the recirculation tank to account for the sample volume used to measure the permeate flux. The average concentration is estimated using:

$$C_{FC} = \frac{1}{2}\left(C_{FR} + \frac{C_{FR}V_{DV}}{(V_{DV} - V_P)}\right) \tag{7d}$$

where V_{DV} is the deadvolume of the system and V_P is the volume of permeate collected during a flux measurement.

Modelling of Experimental Data

The Spiegler-Kedem/Film Theory (SK-FT) model (34) was used to determine membrane transport parameters, σ and P_m. The reflection coefficient, σ, which represents the rejection capability of a membrane (i.e., $\sigma = 0$ for no rejection and $\sigma = 1$ for 100% rejection). Spiegler-Kedem showed that σ represents the fractional contribution of the "defect" free portion of the membrane to the total flow. P_m is the solute permeability:

$$\frac{R_m}{1-R_m} = a_1[1-\exp(-J_v a_2)] \tag{8}$$

$$a_1 = \frac{\sigma}{1-\sigma} \tag{9}$$

$$a_2 = \frac{1-\sigma}{P_m} \tag{10}$$

and R_m is the solute separation based on the wall concentration. Murthy and Gupta (35,36) combined the SK model with film theory:

$$\frac{R_o}{1-R_o} = \frac{R_m}{1-R_m}[\exp(-J_v/k)] \tag{11}$$

where k is the mass transfer coefficient, to describe solute separation based on the observed rejection, R_o, using the average feed concentration of the solute. Combining Eqs. (8) and (11) yields:

$$\frac{R_o}{1-R_o} = a_1[1-\exp(-J_v a_2)][\exp(-J_v/k)] \tag{12}$$

which will henceforth be termed the SK-FT model. Using a nonlinear parameter estimation method (DataFit I and Sigma Plot 10) and the data of observed rejection (R_o) and the solvent flux (J_v) taken at given pressure, the membrane parameters σ and P_m, and mass transfer coefficient, k can be estimated, simultaneously. Murthy and Gupta (35,36) noted that as σ approaches unity, the SK-FT model approaches the Kimura-Sourirajan Analysis model which they had also combined with film theory to yield (35–37):

$$\frac{R_o}{1-R_o} = \frac{J_v}{D_{am}K/\delta}\exp(-J_v/k) \tag{13}$$

where $D_{am}K/\delta$ is a solute transport parameter ($m\,s^{-1}$) and Eq. (13) is henceforth designated as the KSA-FT model. It is worth noting that the more important consideration for the similarity of the SK-FT and KSA-FT models is when the product $J_v(1-\sigma)/P_m$ is sufficiently small, for example <0.01. This can be encountered when J_v is small and/or P_m is large in addition to σ approaching unity. In this situation the SK-FT model reduces to:

$$\frac{R_o}{1-R_o} = \left(\frac{\sigma}{1-\sigma}\right)\left(\frac{J_v(1-\sigma)}{P_m}\right)\exp(-J_v/k) \approx \left(\frac{J_v\sigma}{P_m}\right)\exp(-J_v/k) \tag{14}$$

and $\sigma/P_m \approx \delta/D_{am}K$, with the obvious approximation that $P_m \approx D_{am}K/\delta$ as σ generally approaches unity. This equation can be rearranged and linearized as a function of J_v to:

$$\ln\left(\frac{R_o}{(1-R_o)J_v}\right) = \ln\left(\frac{1}{P_m}\right) - \frac{J_v}{k} \approx \ln\left(\frac{1}{D_{am}K/\delta}\right) - \frac{J_v}{k} \tag{15}$$

with P_m approximated by the intercept and k by the inverse of the slope. In the case of reverse osmosis with low permeate fluxes and/or high mass transfer coefficients, the ratio J_v/k can also become <0.01, concentration polarization can become negligible. This leads to the further simplification such that:

$$\frac{R_o}{1-R_o} = \left(\frac{J_v}{P_m}\right)\exp(-J_v/k) \approx \left(\frac{J_v}{P_m}\right)\left(1-\frac{J_v}{k}\right) \approx \frac{J_v}{P_m} \approx \frac{J_v}{D_{am}K/\delta} \tag{16}$$

which is, simply the KSA-FT model. Spiegler and Kedem also identified the limiting case when J_v approaches zero and the slope of R_o or $R_o/(1-R_o)$ becomes constant and equal to σ/P_m. The importance of this analysis is to determine what regime the membrane process is occuring in and if it is logical to use the KSA-FT or SK-FT models to estimate either k or σ.

RESULTS AND DISCUSSION

Effect of Changes in Feed Water Temperature and Pressure on Permeance in Reverse Osmosis of Pure Water

The pure water permeance before and after correction for the viscosity to 20°C using Eq. (2), are shown in Figs. 1a and 1b respectively. The error bars are generally quite small. At a fixed temperature, the permeance, L, changed only slightly (less than 10%) as the transmembrane pressure was increased from 2 to 5 MPa, with the effect being greater at higher temperatures. However, the viscosity corrected permeance increased significantly with increasing temperature, Fig. 1b. For example, at 2 MPa the corrected permeance increased from 1.95×10^{-11} m/sPa to 2.84×10^{-11} m/sPa, a 46% increase, when the temperature was increased from 20 to 50°C. These results suggested that temperature changes affecting the viscosity of water, due to the decreasing Newtonian or bulk viscosity are not the only factors leading to an increase in flux. The coefficients of variation, CoV, (i.e., standard deviation/mean) were found to be very small. The temperature and

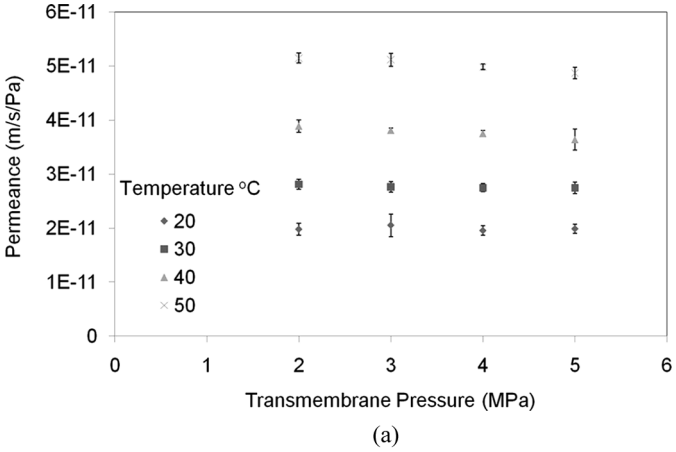

(a)

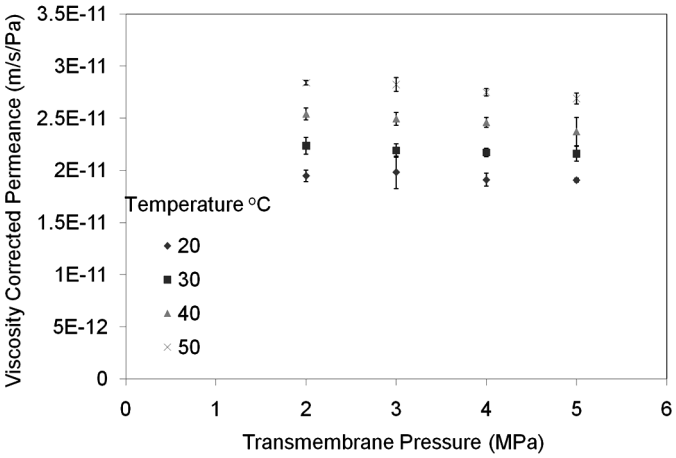

(b)

FIG. 1. RO studies with pure water; a) Permeance vs transmembrane pressure with pure water, b) Viscosity corrected permeance using Eq. (2) against transmbrane pressure with pure water at a range of temperatures. The coefficients of variation, CoV, (i.e., standard deviation/mean) were very small. With the pure water studies, the sequence of cyclic pressure changes (i.e., up or down) had no effect on the permeance (i.e., no hysteresis effect).

pressure effect experiments were performed in an up and down sequence. We can argue that a better way would have been to perform these experiments in random order to avoid any systematic error in the experiments. While this was not done in this study, the small error bars (Figs. 1a and 1b) suggest that the experimental inaccuracy resulting from the current systematic sequence was not significant.

The temperature dependence of the permeate flux is also depicted in Fig. 2 where it was normalized by the average flux at 20°C using Eq. (1). The results in this work were very close to that reported by Sharma et al. (26) (data generated using Eq. 1). The temperature dependence in this work was 3118 ± 150 K, as measured by the slope, and was not statistically different from Sharma's result.

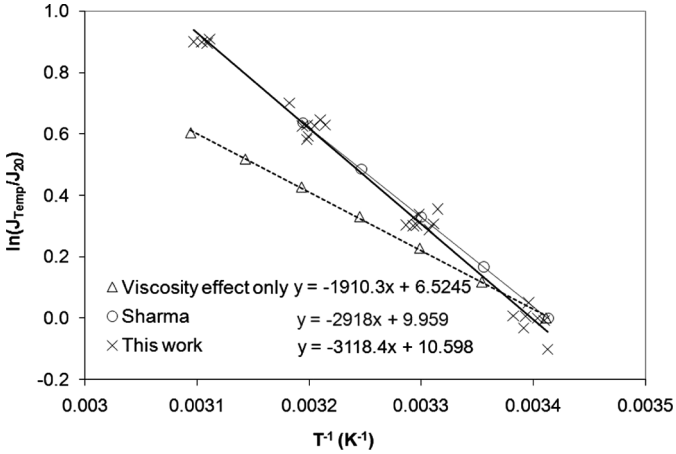

FIG. 2. Temperature dependence of the flux normalized by pressure, viscosity and the average flux at 20°C and 20 bar. Also shown are the predictions according to Sharma et al. (2003) and the effect of temperature via the Newtonian viscosity alone. Note there is a direct overlap of the current work results with Sharma et al.'s results (upper line).

Although the membranes were from different manufacturers, they were both RO rated polyamide thin film composites (TFC), hence the similarities may be expected. While the comparison with Sharma et al.'s (26) reference is useful to show, it is important to point out that this work was based on TFC NF membranes and not TFC SWRO membranes. Furthermore, while the permeate flux increased with both transmembrane pressure and feed temperature, in the case of the pure water studies the sequence of cyclic pressure changes (i.e., up or down) had no apparent effect on the permeance at a given temperature (i.e., no hysteresis effect).

Activated Pure Water Transport Mechanisms & Temperature Induced Morphological Changes

The strong dependence of the permeance on the temperature suggests that the viscosity corrections do not account for the flux increases at higher temperatures. The data in Fig. 1b should be co-linear if the viscosity corrections were adequate and there were no morphological changes in the membrane itself. Comparing the uncorrected permeance data (Fig. 1a) with the viscosity corrected permeance (Fig. 1b) shows that the viscosity changes accounted for a significant portion, though not all, of the increase in permeance due to changes in the temperature. This also assumes that the viscosity correction equation (Eq. 2) is accurate. The implication of Fig. 1b is that the physical properties of the membrane change with temperature. The fact that the corrected permeance was always highest at 50°C and lowest at 20°C, irrespective of the sequence in which the temperature experiments were run (i.e., up or down), indicates that the change occuring in the permeability of the membrane is reversible.

As Sharma and Chellam (49) reported in their work on temperature effects on the morphology of porous thin film composite nanofiltration membranes, changes in membrane morphology at higher temperatures would be expected to increase the permeance as the polymers would soften slightly and be susceptible to creep, compaction, or mild annealling/coalescence of the pores. In similar temperature cycling experiments, Manttari et al. (23) reported irreversible decreases in permeance for most of the nanofiltration membranes they evaluated during processing of glucose solutions (250 ppm) after the membranes were used at 65°C. The permeance loss was greatest for the membranes with the lowest temperature ratings, as could be expected. The composite polyamide RO membrane used in our studies had a maximum operating temperature rating of 45°C and maximum operating pressure rating of 83 bar based on the manufacturer's specifications. In the current work we were well within the maximum pressure limit and only slightly above the maximum operating temperature limit.

Compaction is evident in Figs. 1a and 1b by the negative slopes, the most significant case, as expected at 50°C. The time effect might also be important when compaction is studied. Therefore in some experiments the RO unit was run for one to two hours. Permeate samples were then taken. The same results were obtained as with the shorter run times. The temperature of 50°C and pressure of 50 bar means that the so-called Wagner unit (i.e., temperature × pressure) is 2500. A value greater than 2000 means that it is rarely possible to avoid compaction (38).

The viscosity correction assumes that Newtonian flow still applies at sub-nanometer pore dimensions. At this scale the existance of water clusters must be considered. Nemethy and Scheraga (39) reported water clusters containing ~91 and ~25 water molecules at 0°C and 90°C respectively, which yield cluster radii of ~0.87 nm and ~0.56 nm respectively, when using a molecular volume of 0.0299 nm^3. These clusters are in equilibrium with non-clustered water and have very short lifetimes (10^{-10}–10^{-11} seconds). The potential impact of water cluster size on the temperature dependence of the permeance can be made by considering the effective viscosity of water in the membrane to be inversely proportional to the cluster size. Schultz and Asunmaa (40) also estimated the effective viscosity of water in RO membranes.

Bowen and Yousef (41) studied the permeation of various salts in nanofiltration (NF) membranes. They found that the addition of a salt resulted in a higher flux. This was attributed to the salts "breaking up" the water structures in the small pores and was reported as a reduction in the effective viscosity of the water, as the absolute value of the viscosity could not be determined. A thorough treatment of the effects of temperature on water permeance in thin film composite nanfiltration membranes was also reported by Sharma et al. (26) They found that increasing temperature increased the mean pore radii and the molecular weight cutoff suggesting changes in the structure and morphology of the polymer matrix comprising the membrane barrier layer. They noted that there was a need to develop separate expressions for temperature correction of the flux for individual membranes to accurately normalize water productivity observed over a range of temperatures.

Arrhenius plots of viscosity-corrected water permeance across the SWC1–2540 RO composite polyamide membrane for this study (data not shown) gave an activation energy of -8.6 ± 1.2 kJ/gmol for the non-viscous contributions to flow, comparing very well with an average value of -8.1 kJ/gmol from Mehdizadeh and Dickson (42) for the SW30HR membrane in the 5–40°C temperature range. Sharma et al. (26) reported an activation energy of -6.4 ± 0.9 kJ/gmol for the non-viscous contributions to water transport.

The effect of temperature on morphological changes can result in swelling or plasticization. Plasticization is not expected at 50°C as the glass transition temperature for aromatic polyamides ranges from 90 to 425°C (43). If changes in the pure water flux, after correction for the water viscosity, were attributed to swelling, an estimate of the relative change in pore radius can be estimated. It is assumed that the pore radius is proportional to the radius of polymer nodules in the skin layer (40) and that the Hagen Poiseuille flow applies. The relative change in the pore radius for all pressures and temperatures can be estimated from the pressure and viscosity normalized flux (Eq. 17):

$$\frac{r_{pT}}{r_{p20}} = \left(\frac{J_{VT}}{J_{V20}}\frac{\Delta P_{20}}{\Delta P_T}\frac{\mu_T}{\mu_{20}}\right)^{1/4} \tag{17}$$

The predicted relative increases in pore radius required to account for the observed pure water flux, after accounting for viscosity changes of the water, are shown in Fig. 3. At 50°C 8% swelling would be required; this is approximately two orders of magnitude greater than predicted using a thermal expansion coefficient of $5 \times 10^{-5}\,K^{-1}$ for a typical polymer (symbol × in Fig. 3). Hence it would appear that non-viscous changes in the pure permeance of the SWC1 membrane are not related to physical changes of the membrane.

Estimation of σ, P_m and k From the SK-FT & KSA-FT Models in Reverse Osmosis of Saline Solutions

The permeance during the 4% NaCl tests, after correcting for the temperature dependence of the permeate viscosity and the osmotice pressure of the feed using Eq. (4), is shown in Fig. 4 for the up and down temperature cycle.

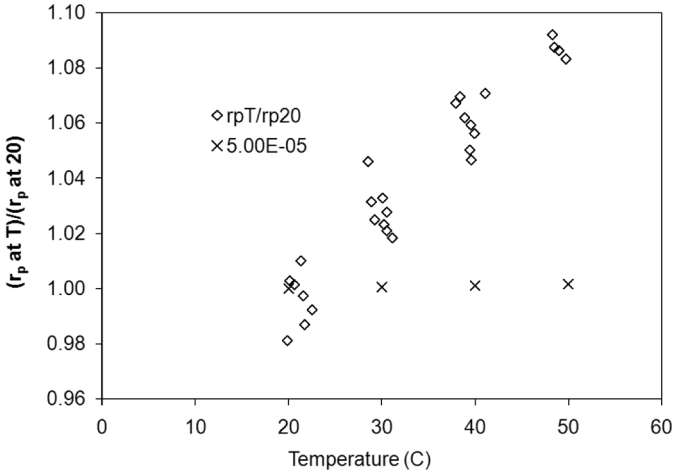

FIG. 3. Predicted relative increases in effective pore radius required to account for pure water flux increases beyond changes to water viscosity. The symbol X refers to predicted relative increases in effective pore radius using a typical polymer thermal expansion coefficient of $5 \times 10^{-5}\,\mathrm{K}^{-1}$. (Note that temperature for x axis is in °C).

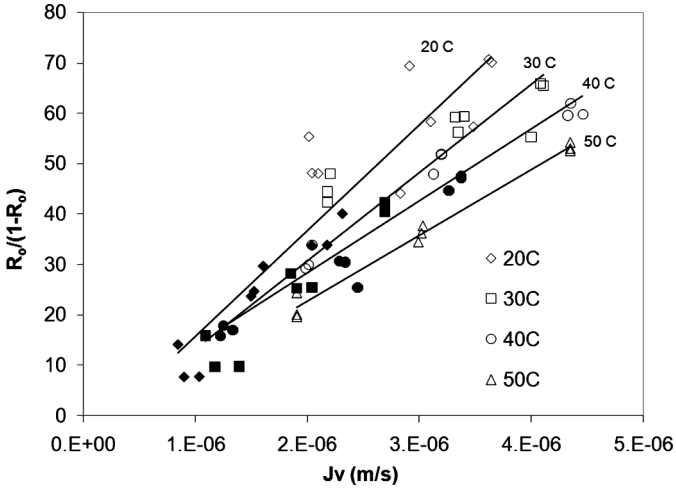

FIG. 5. Experimental $R_o/(1-R_o)$ as a function of the flux, J_V, for each temperature. Solid black symbols of the same shape indicate data during the temperature downswing, white symbols refer to the up sequence. Solid lines are straight line fits, only used to help visualize data at the different temperatures. (temperature in °C).

There appears to be a decline in the permeance after operating at 50°C. However, this decline is not statistically significant when the 95% confidence intervals are considered, as all the probable values overlap. Variations in the magnitude of the error is primarily associated with errors in the estimation of the osmotic pressure of the feed, rather than errors in measurement of the permeation rate itself.

Assuming negligible conentration polarization effects (i.e., $J_v/k < 0.01$), the changes in the experimantal values of the observed rejection, in the form $R_o/(1-R_o)$, may be plotted as a function of flux, J_v, using Eq. (16) the simplified form of the KSA-FT or the SK-FT model (Fig. 5). The observed rejection was well correlated by J_v. The observed rejection during the upswing (open symbols in Fig. 5) are co-linear with those during the downswing, suggesting no changes to the membrane itself as a result of the temperature or pressure changes. Fluxes in the downswing tended to be lower as the feed concentration was higher during these experiments.

All the data sets were also examined using the linearized form of the KSA-FT model (Eq. 15). Two typical data sets are shown in Fig. 6 for a temperature upswing and

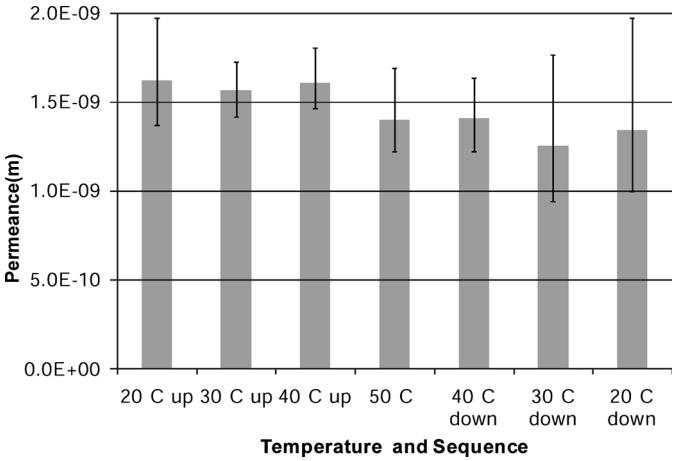

FIG. 4. Corrected permeance, L, in m/sPa, for 4% (w/v) saline water at a range of temperatures using two up temperatute sequences. The indication to "up" and "down" refers to the temperature sequence, whether the temperature was being increased or decreased at that stage of the experiment. Permeance was calculated using Eq. (4) and the effective transmembrane pressure drop (i.e., operating or average pressure minus the osmotic pressure) (Note that temperature for x axis is in °C).

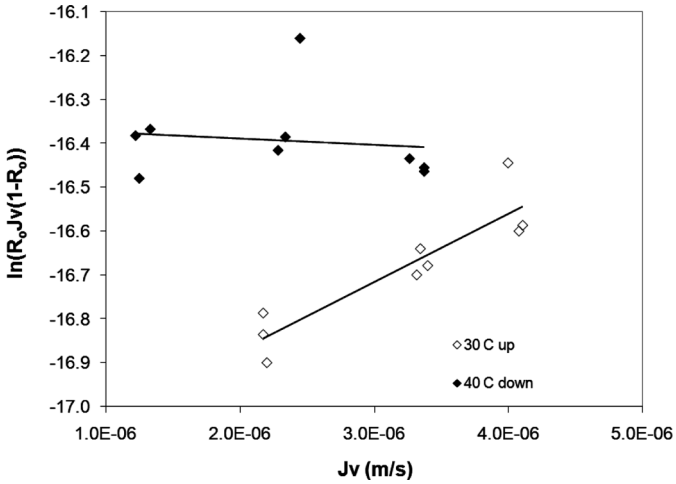

FIG. 6. Graphical presentation of linearized form of KSA-FT model (Eq. 15) for two experimental data sets. Solid lines are from the model and open and closed squares are the observed data. (Note that temperature for x axis is in °C).

TABLE 1
Estimates of σ, P_m, $D_{am}K/\delta$ and k for up (U) and down (D) temperature cycles

T°C	$-\text{LOG}(1-\delta)$	σ (−)	P_m SK-FT (m/s)	$D_{am}K/\delta$ KSA-FT (m/s)	k SK-FT (m/s)	k KSA-FT (m/s)
20 U	4.37	1.00	2.94E–08	2.85E–08	5.75E–06	5.32E–06
30 U	4.33	1.00	3.45E–08	3.46E–08	6.49E–06	6.47E–06
40 U	6.44	1.00	5.35E–08	5.73E–08	1.54E–05	2.16E–05
50	6.26	1.00	8.28E–08	8.34E–08	9.79E + 00	−2.69E–05
40 D	6.39	1.00	7.47E–08	7.85E–08	1.26E + 01	−6.94E–05
30 D	6.17	1.00	7.09E–08	7.18E–08	1.20E + 00	−3.68E–06
20 D	5.95	1.00	6.25E–08	5.87E–08	2.36E + 04	−2.90E–06

downswing. The 30°C upswing data set follows the expected trend for the KSA-FT model. The 40°C downswing data set on the other hand has a slightly negative slope, predicting a negative mass transfer coefficient. Statistically the slope encompasses zero suggesting that concentration polarization is not significant and that only the parameter $D_{am}K/\delta$ can be estimated. This is consistent with the earlier disussions where data at higher temperatures and or lower J_v are in the range where the SK-FT model is linear with respect to J_v, that is, the concentration polarization mass transfer is not significant.

The estimates of $D_{am}\text{K}/\delta$, P_m, σ, and k for the two models are summarized in Table 1. Values of the reflection coeffient, σ, are almost unity for all cases (indicating close to 100% rejection of solute) and so σ is transformed using $-\log_{10}(1-\sigma)$ to facilitate comparisons. There is no smooth variation of σ during the temperature upswing. Overall, σ, increases with increasing temperature, although one can argue that there are two finite values, one at 20 and 30°C and another at 40 and 50°C suggesting that a change occurred in the membrane. One can conjecture on the expected behavior of σ with increasing temperature. Spiegler and Kedem (34) described σ as the ratio of solute transport by the "perfect membrane" to the total flow, or $1-\sigma$ is the ratio of solute transport by "leaks" (convection) to the total flow. Hence any temperature effect would reflect the relative importance of these two transport mechanisms. Let us assume that leaks represent solute transport by convection, hindered or not, and transport by the perfect portion of the membrane is to be via P_m.

A reflection coefficient, σ, close to 1 does not indicate a non-porous membrane, rather it means that permeation is via a solution-diffusion mechanism, the combination of which yields the permeability. The use of the Hagen Poiseuille Eq. (17) to estimate pore size appears to be inconsistent with this observation. However, we are not attempting to approximate the pore size but rather the expected change in the pore dimensions, if there were any, which would account for the increased flux, after viscosity changes were also accounted for. What was shown with Eq. (17) (Fig. 3) is that thermal expansion could not account for the increased permeability. We can speculate based on our discussion of the water cluster size/temperature, that it is the water that is changing beyond normal viscosity effects, that is yielding the higher permeation. Further to this point, a reflection coefficient of unity implies a defect free membrane in the context that solute transport is not simply by convection with zero rejection. This does not mean that there are no pores. Sharma et al. (26) and Sharma and Chellam (29,30,49) also showed incomplete rejection for many solutes. Even dense films of gas separation membranes are recognized as having pores (50).

Table 1 shows distinctly different P_m and DK/δ values for up and down sequence experiments for the same temperature. Data reported in Table 1 and Fig. 7 suggests that changes in membrane performance may not be reversible. In addition, if feed concentration changed significantly

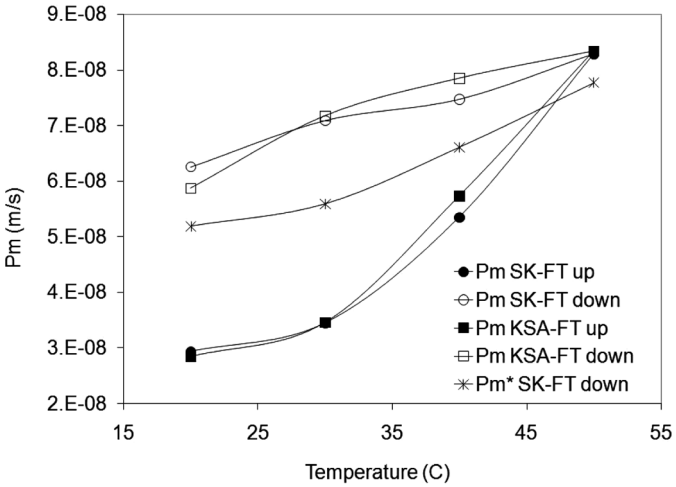

FIG. 7. NaCl permeability, P_m, as determined using the SK-FT and KSA-FT models. KSA-FT values for up and down sequences. (temperature in °C).

during up and down experiments (which can lead to two different solute permeability values) then it may be the result of an experimental error which can confound data interpretation.The solute permeability calculated using SK-FT and KSA-FT models are independent of flux and pressure and should remain constant if cyclic effects are completely reversible. In addition, solute permeability values reported in Table 1, as well as in Fig. 7, for down experiments are always higher compared to up experiments (especially for low 20 and 30°C runs) and may be interpreted as a hysteresis or memory effect on membrane permeability (46–48). This is in contrast to the pure water studies where no hysteresis was observed. For the saline water studies, however, the membrane may remember its previous physical state and as such a delay occurs between the application and the removal of a force and its ensuing effects. We can argue that this is similar to elastic hysteresis observed in the effects of loading/unloading on the extension of a rubber band. Elastic hysteresis was one of the first types of hysteresis to be examined (47). Let us take a closer look at this phenomenon and see how it may explain the hysteresis observed in our saline water membrane permeability results with the up/down sequences.

Hysteresis phenomena occur in magnetic materials, ferromagnetic materials, and ferroelectric materials, as well as in the elastic, electric, and magnetic behavior of materials, in which a lag occurs between the application and the removal of a force or field and its subsequent effect (i.e., memory effect) (46–48). A way to understand it is in terms of a rubber band with weights attached to it. As weights are loaded onto it, the band will extend because the force the weights are exerting on the band is increasing (i.e., comparable to increasing temperature in the membrane in the up cycle in Fig. 7). As the weights are taken off, each weight that produced a specific length as it was loaded onto the band now produces a slightly longer length as it is unloaded (i.e., compared to decreasing temperature in down cycle). This is because the band does not obey Hooke's law (i.e., strain is directly proportional to stress) perfectly. We can relate this elastic hysteresis effect to what was observed in our membrane system (Table 1, Fig. 7). At a specific temperature, the down temperature cycle (i.e., decreasing loading) results in a more permeable membrane (i.e., higher P_m and higher DK/δ) than the up cycle. The former can be compared to the slightly longer length of the elastic band as it is unloaded, and is due to the "memory" that the membrane material has of its previous physical condition (i.e., higher temperature). However, we must point out that the membrane permeability hysteresis effect due to cyclic changes in temperature and pressure is not well understood and is one area where further work is needed. For example, why did we observe membrane hysteresis with the saline water studies but not with the pure water studies?

If the permeability of a solute is taken as an analogue to gas permeability, the product of the solubility and diffusivity in the membrane skin layer, then the increasing P_m with increasing temperature would be expected. There was an overall NaCl feed concentration increase during the experiments, which may suggest a concentration dependence of P_m. However, Murthy and Gupta (37), in their experiments with CA RO membranes, showed very little variation (<1%) of P_m, with either model, over a 30-fold increase in concentration (1,000 to 30,000 ppm). Their values of P_m were $\sim 4.7 \times 10^{-7}$ m/s (KSA-FT) and 4.1×10^{-7} m/s (SK-FT), at 25°C, considerably larger than the values 3×10^{-8} and 6×10^{-8} m/s found in this work (at 20°C) with a polyamide skin layer. Hence, in the absence of any defects, a polyamide membrane would have higher NaCl rejection.

It is possible to use the estimated solute permeability, P_m, data to study the activation energy, E_a, associated with solute transport across the RO membrane (44). The dependence of P_m on temperature shown in Fig. 7 can be expressed by an Arrhenius type equation:

$$P_m \propto \exp(-E_a/RT) \tag{18}$$

where R is the gas constant and E_a is the activation energy associated with the solute permeability. A plot of Ln P_m against $1/T$ follows the form "$y = mx$" and should be a straight line with a slope equal to $-E_a/R$ from which the activation energy may be obtained. The data from Fig. 7 were replotted as shown in Fig. 8. Activation energies, E_a, for solute permeability in transport of NaCl through the RO membrane were determined to be

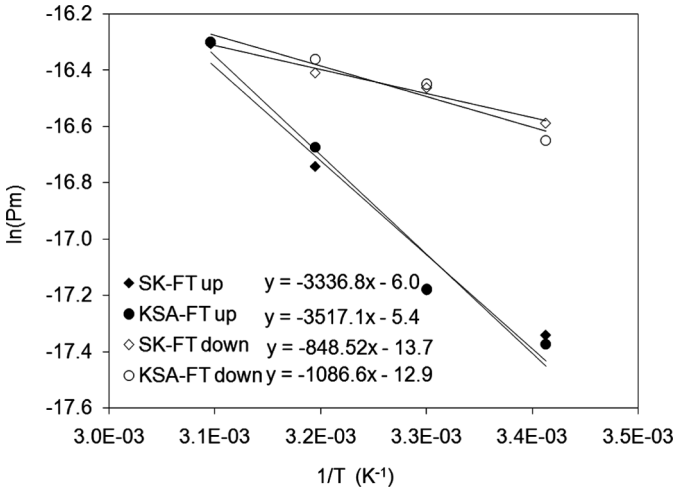

FIG. 8. Arrhenius plots for the NaCl permeability for up and down temperature cycles shown in Fig. 7. A plot of Ln P_m against $1/T$ follows the form "$y = mx$" and should be a straight line with a slope equal to $-E_a/R$ from which the activation energy may be obtained.

TABLE 2
Mass transfer coefficients relative to 20°C, experimental and predicted values

Temperature °C	K (m/s)	k_T/k_{293} Experimental (−)	k_T/k_{293} Predicted by Eq. (19) (−)
20	5.75E−06	1.0	1.0
30	6.49E−06	1.1	1.3
40	1.54E−05	2.7	1.7
50	5.62E−05	9.8	2.2

27.7 ± 4.3 kJ/gmol and 29.2 ± 3.8 kJ/gmol on the temperature upswing cycle for the SK-FT and KSA-FT models respectively. These compared to 25.9 kJ/gmol for the activation energy of pure water flow in these membranes. The slope or temperature dependence maybe similar, but the intercept and hence the absolute value are quite different. On the temperature downswing the activation energies, E_a, were 7.1 ± 0.7 and 9.0 ± 1.6 kJ/gmol respectively. The statistically significant differences in activation energy reported for NaCl permeation during the up and down experiments (Fig. 8) suggest that experiments during up and down cycles were not completely reproducible. However, the lower E_a values could also mean temporary changes in membrane morphology (i.e., more permeable membrane due to an elastic hysteresis or memory effect as explained above) which made it easier for the solute to pass through the membrane.

The expected dependence of the mass transfer coefficient, k, on temperature can be quantified using correlations (45). In turbulent flow, $k \propto D^{2/3}/\mu^{1/2}$ while in laminar flow $k \propto D^{2/3}$ where $D \propto T_{abs}/\mu$. In turbulent flow a greater temperature dependence would be expected because of both diffusivity increases and viscosity decreases. Assuming that the viscosity dependence of the salt solutions on temperature is similar to that of water, then the relative changes in the mass transfer coefficient could be expected to follow:

$$\frac{k_T}{k_{293}} = \left(\frac{T}{293}\right)^{2/3} \left(\frac{\mu_{293}}{\mu_T}\right)^{7/6} \tag{19}$$

As shown in Table 2, the relative increase in the experimentally observed mass transfer at increasing temperatures is much greater than predicted by Eq. (19). The error is moderate at 30 and 40°C but extreme at 50°C, when the experimentally predicted relative k is ~4.5 times greater than expected.

In summary, the overall effects of cyclic changes in operating temperature and pressure on permeation properties of composite polyamide RO membranes can be represented by Fig. 9. Increasing feed/operating temperatures increases movement of polymer chains and hence increases membrane porosity. In addition, the higher temperatures decrease water/solute cluster size which in turn lowers viscosity. Both of these increase permeance and decrease rejection. Increasing transmembrane pressure, on the other hand, may cause membrane compaction, resulting in lower permeance. The net effect on permeance and retention is a combination of these factors. The permeance, for example, is greatest and the solute rejection lowest under operating conditions of high temperature and low pressure (case B).

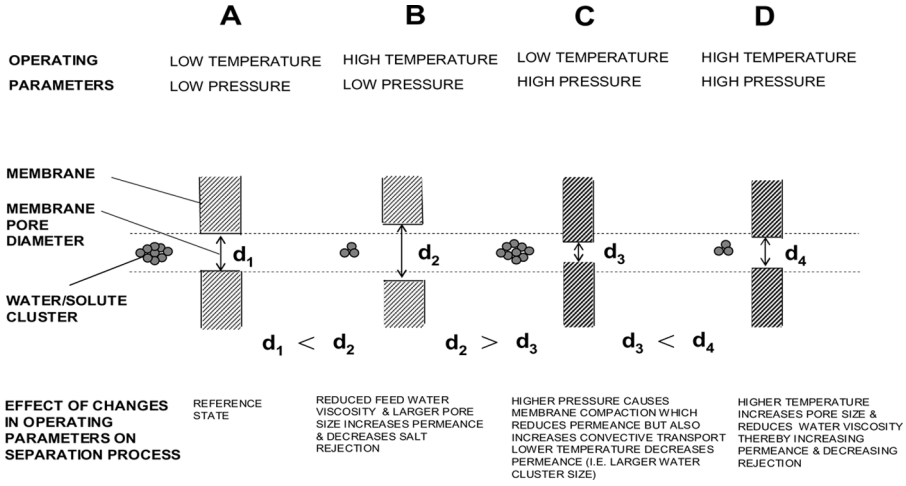

FIG. 9. Graphical representation of effects of cyclic changes in operating temperature and pressure on permeation properties of composite polyamide RO membranes.

CONCLUDING REMARKS

The results of this study indicate that the changes occurring in the permeability of the membrane were reversible since the viscosity corrected permeance was always highest at 50°C and lowest at 20°C, irrespective of the cyclic up or down sequence in which the temperature experiments were run. In the case of the pure water studies the sequence of cyclic pressure changes (i.e., up or down) had no apparent effect on the permeance at a given temperature (i.e., no hysteresis effect). The changes in the observed rejection appear to be consistent with the Spiegler-Kedem/ Film Theory (SK-FT) and the Kimura-Sourirajan Analysis/ Film Theory (KSA-FT) models. While concentration polarization was not shown to be significant, the permeability of NaCl, P_m in the SK-FT model or $D_{am}K/\delta$ in the KSA-FT model, showed a strong temperature dependence increasing from 3×10^{-8} m/s at 20°C to 8.3×10^{-8} m/s at 50°C. Some compaction was suggested at the higher pressures as shown by the hysteresis in the up/down cyclic temperature and pressure experiments with saline water and may be interpreted as a "memory" that the membrane material has of its previous physical condition. However, no permanent membrane damage was observed in any of the studies. The overall results suggest that the net effect on permeance and solute rejection is the consequence of several interactions with feed/operating temperatures affecting membrane porosity and water/ solute cluster size, and transmembrane pressure influencing membrane compaction. The outcomes of this investigation imply that cyclic changes in the operating temperature and pressure should not damage the spiral wound composite polyamide seawater reverse osmosis, thus allowing for longer membrane lifetimes.

ACKNOWLEDGEMENTS

We are thankful to the Middle East Desalination Research Centre (Contract Number 97-A-2001) and Sultan Qaboos University (IG/AGR/BIOR/01/02) for financial support. The assistance of D. Jackson (Imperial College, UK) and M. Al-Belushi and S. Al-Maskri (SQU, Oman) is greatfully acknowledged.

NOMENCLATURE

a_1	constant
a_2	constant
C_{FC}	salt concentration of corrected feed (ML^{-3})
C_P	salt concentration in permeate (ML^{-3})
C_{Fi}	initial feed concentration (ML^{-3})
C_{Fo}	outlet feed concentration (ML^{-3})
C_{FC}	salt concentration of corrected feed (ML^{-3})
C_{FR}	salt concentration recovered in module (ML^{-3})
D	diffusion coefficient (L^2T^{-1})
$D_{am}K/\delta$	solute transport parameter (LT^{-1})
E_a	Arrhenius activation energy associated with solute flux through membrane (kJ/mole)
$J_{V,T}$	volumetric flux at temperature T (LT^{-1})
J_V	volumetric flux (LT^{-1})
k	mass transfer coefficient (LT^{-1})
L	permeance (i.e., flux/pressure) (L^2TM^{-1})
N	number of clusters
P_m	solute permeability (LT^{-1})
P	pressure ($ML^{-1}T^{-2}$)
$\triangle P$	transmembrane pressure ($ML^{-1}T^{-2}$)
Q_F	retentate flow rate at inlet (L^3T^{-1})
Q_P	retentate flow rate at outlet (L^3T^{-1})
R	the gas constant (8.3145 J mol^{-1} K^{-1})
R_m	solute separation based on wall concentration
R_o	observed rejection
r_P	pore radius (L)
r_{PT}	pore radius at temperature T (L)
S	conductivity (SL^{-1}) (note: The basic unit of conductivity is the siemens (S))
SSR	sum of squares of residuals
T	temperatute (K or °C)
V_{DV}	dead volume (L^3)
V_P	volume of permeate collected during flux measurment (L^3)

Greek

Π_{FW}	osmotic pressure of feed at membrane wall
Π_P	osmotic pressure of permeate
σ	reflection coefficient
μ	viscosity ($ML^{-1}T^{-1}$)
ν	kinematic viscosity (viscosity/density) (L^2T^{-1})
τ	effective pore length (L)
ρ	density (ML^{-3})
ε	surface porosity

REFERENCES

1. Zhao, Y.; Song, L.; Ong, S.L. (2010) Fouling behaviour and fouling characteristics of reverse osmosis membranes for treated secondary effluent reclamation. *J. Membr. Sci.*, 349 (1–2): 65–74.
2. Singh, R.; Tembrock, J. (1999) Effectively controlled reverse osmosis systems. *Chemical Engineering Progress*. September: 57–66.
3. Al-Sajwani, T.M.A. (1998) The desalination plants of Oman: Past, present and future. *Desalination*, 120: 53–59.
4. Niewersch, C.; Meier, K.; Wintgens, T.; Melin, T. (2010) Selectivity of polyamide nanofiltration membranes for cations and phosphoric acid. *Desalination*, 250 (3): 1021–1024.
5. Goosen, M.F.A.; Al-Hinai, H.; Sablani, S. (2001) Capacity-building strategies for desalination: Activities, facilities and educational programs in Oman. *Desalination*, 141: 181–189.
6. Goosen, M.F.A.; Sablani, S.S.; Al-Maskari, S.S.; Al-Belushi, R.H.; Wilf, M. (2002) Effect of feed temperature on permeate flux and mass transfer coefficient in spiral-wound reverse osmosis systems. *Desalination*, 144: 367–372.
7. Goosen, M.F.A.; Shayya, W.H. (1999) Water Management, Purification and Conservation in Arid Climates. In: *Water Management, Purification and Conservation in Arid Climates; Vol. 1, Water*

Management, Goosen, M.F.A.; Shayya, W.H., eds.; Technomic: Lancaster, PA, USA, 1–6.
8. Ahmed, M.; Arakel, A.; Hoey, D.; Thumarukudy, M.R.; Goosen, M.F.A.; Al-Haddabi, M.; Al-Belushi, A. (2003) Feasibility of salt production from inland RO desalination plant reject brine: A case study. *Desalination*, 158: 109–117.
9. Mahmoudi, H.; Spahis, N.; Goosen, M.F.; Sablani, S.; Ghaffour, N.; Drouiche, N. (2009) Assessment of wind energy to power solar brackish water greenhouse desalination units: A case study from Algeria. *Renewable and Sustainable Energy Reviews*, 13 (8): 2149–2155.
10. Tahri, T.; Abdul-Wahab, S.A.; Bettahar, A.; Douani, M.; Al-Hinai, H.; Al-Mulla, Y. (2009) Simulation of the condenser of the Seawater Greenhouse, Part II: Application of the developed theoretical model. *J. Thermal Analysis and Calorimetry*, 96: 43–47.
11. Rahimpour, A.; Jahanshahi, M.; Mortazavian, N.; Madaeni, S.S.; Mansourpanah, Y. (2010) Preparation and characterization of asymmetric polyethersulfone and thin-film composite polyamide nanofiltration membranes for water softening. *Applied Surface Science*, 256 (6): 1657–1663.
12. Penkova, A.V.; Polotskaya, G.A.; Gavrilova, V.A.; Toikka, A.M.; Liu, J.-C.; Trchova, M.; Slouf, M.; Pientka, Z. (2010) Polyamide membranes modified by carbon nanotubes: Application for pervaporation. *Separation Science and Technology*, 45: 35–41.
13. Sridhar, S.; Kalyani, S.; Ravikumar, Y.V.L.; Muralikrishna, T.S.V.N. (2010) Performance of composite membranes of poly(ether-*block*-amide) for dehydration of ethylene glycol and ethanol. *Separation Science and Technology*, 45: 322–330.
14. Nghiem, L.D.; Coleman, P.J.; Espendiller, C. (2010) Mechanisms underlying the effects of membrane fouling on the nanofiltration of trace organic contaminants. *Desalination*, 250 (2): 682–687.
15. Chen, V.; Fane, A.G.; Madaeni, S.; Wenten, I.G. (1997) Particle deposition during membrane filtration of colloids: Transition between concentration polarization and cake formation. *J. Membr. Sci.*, 125: 109–122.
16. Chudacek, M.W.; Fane, A.G. (1984) The dynamics of polarization in unstirred and stirred ultrafiltration. *J. Membr. Sci.*, 21: 145–160.
17. Clifton, M.J.; Abidine, N.; Aptel, P.; Sanchez, V. (1984) Growth of the polarization layer in ultrafiltration and hollow-fibre membranes. *J. Membr. Sci.*, 21: 233–246.
18. Dal-Cin, M.M.; MeLellan, F.; Striez, C.N.; Tam, C.M.; Tweddle, Kumar, A. (1966) Membrane performance with a pulp mill effluent: Relative contributions of fouling mechanisms. *J. Membr. Sci.*, 120: 273–285.
19. Denisov, G.A. (1994) Theory of concentration polarization in cross-flow ultrafiltration: Gel-layer model and osmotic-pressure model. *J. Membr. Sci.*, 91: 173–187.
20. Ghayeni, S.B.S.; Beatson, P.J.; Schncider, R.P.; Fane, A.G. (1998) Adhesion of waste water bacteria to reverse osmosis membranes. *J. Membr. Sci.*, 138: 29–42.
21. Sablani, S.S.; Goosen, M.F.A.; Al-Belushi, R.; Gerardos, V. (2002) Influence of spacer thickness on permeate flux in spiral-wound seawater reverse osmosis systems. *Desalination*, 146: 225–230.
22. Koltuniewicz, A.; Noworyta, A. (1994) Dynamic properties of ultrafiltration systems in light of the surface renewal theory. *Industrial Engineering and Chemical Research*, 33: 1771–1779.
23. Manttari, M.; Pihlajamaki, A.; Kaipainen, E.; Nystrom, M. (2002) Effect of temperature and membrane pre-treatment by pressure on the filtration properties on nanofiltration membranes. *Desalination*, 145: 81–86.
24. Katarzynski, D.; Staudt, C. (2010) Temperature-dependent separation of naphthalene/*n*-decane mixtures using 6FDA–DABA-copolyimide membranes. *J. Membr. Sci.*, 348 (1–2): 84–90.
25. Arsuaga, J.M.; López-Muñoz, M.J.; Aguado, J.; Sotto, A. (2008) Temperature, pH and concentration effects on retention and transport of organic pollutants across thin-film composite nanofiltration membranes. *Desalination*, 221 (1–3): 253–258.
26. Sharma, R.R.; Agrawal, R.; Chellam, S. (2003) Temperature effects on seiving characteristics of thin-film composite nanofiltration membranes: Pore size distributions and transport parameters. *J. Membr. Sci.*, 223: 69–87.
27. Nederlof, M.M.; Folmer, H.X.; Verdouw, J.; Heijman, B. (1997) Integrity of membrane elements, vessels and systems. *Desalination*, 113: 179–181.
28. Vazquez, M.I.; Benavente, J. (2003) A study of temperature effect on chemical, structural and transport parameters determined for two different regenerated cellulose membranes. *J. Membr. Sci.*, 219: 59–67.
29. Sharma, R.R.; Chellam, S. (2006) Temperature and concentration effects on electrolyte transport across Porous thin film composite nanofiltration membranes: Pore transport mechanisms and energetics of permeation. *J. Colloid and Interface Science*, 298 (1): 327–340.
30. Sharma, R.R.; Chellam, S. (2008) Solute rejection by porous thin film composite nanofiltration membranes at high feed water recoveries. *J. Colloid and Interface Science*, 328: 353–366.
31. Marquez-Linares, F.; Roque-Malherbe, R.M.A. (2006) Synthesis and characterization of large specific surface area nanostructured amorphous silica materials. *J. Nanosci. Nanotechnol.*, 6 (4): 1–5.
32. Weast, R.C. (Ed) (1979) *Handbook of Chemistry and Physics,* 60th Ed.; CRC Press: Boca Raton, Florida, F51.
33. Lide, D.R. (Ed) (2007) Equivalent Conductivity of Electrolytes in Aqueous Solution. In: *CRC Handbook of Chemistry and Physics, Internet Version*, 87th Ed.; Taylor and Francis: Boca Raton, FL.
34. Spiegler, K.S.; Kedem, O. (1966) Thermodynamics of hyperfiltration (reverse osmosis): Criteria for efficient membranes. *Desalination*, 1: 311–326.
35. Murthy, Z.V.P.; Gupta, S.K. (1997) Estimation of mass transfer coefficient using a combined nonlinear membrane transport and film theory model. *Desalination*, 109: 39–49.
36. Murthy, Z.V.P.; Gupta, S.K. (1997) Sodium cyanide separation and parameter estimation for reverse osmosis thin film composite membrane. *J. Membr. Sci.*, 154: 89–103.
37. Murthy, Z.V.P.; Gupta, S.K. (1996) Simple graphical method to estimate membrane transport parameters and mass transfer coefficient in a membrane cell. *Separation Science and Technology*, 31: 77–94.
38. Paluch, M.; Roland, C.M.; Pawlus, S. (2002) Temperature and pressure dependence of the α-relaxation in polymethylphenylsiloxane. *The Journal of Chemical Physics*, 116 (24): 10932–10937.
39. Nemethy, G.; Scheraga, H.A. (1962) Structure of water and hydrophobic bonding in porteins. I. A model for the thermodynamic properties of liquid water. *The Journal of Chemical Physics*, 36 (12): 3382–3400.
40. Schultz, R.D.; Asunmaa, S.K. (1970) Ordered Water and the Ultrastructure of the Cellular Plasma Membrane. In: *Recent Progress in Surface Science*, Vol. 3, Danielli, J.F.; Riddiford, A.C.; Rosenberg, M., eds.; Academic Press: New York, 291–332.
41. Bowen, W.R.; Yousef, H.N.S. (2003) Effect of salts on water viscosity in narrow membrane pores. *Journal of Colloid and Interface Science*, 264: 452–457.
42. Mehdizadeh, H.; Dickson, J.M. (1991) Modelling of temperature effects on the performance of reverse osmosis membranes. *Chem. Eng. Comm.*, 103: 99–117.
43. Mark, J.E. (Ed) (1999) *Polymer Data Handbook*; Oxford University Press: New York.
44. Godino, M.P.; Barragan, V.M.; Izquierdo, M.A.; Villaluenga, J.P.G.; Seoane, B.; Ruiz-Bauza, C. (2009) Study of the activation energy for transport of water and methanol through a Nafion membrane. *Chemical Engineering Journal*, 152: 20–25.

45. Cheryan, M. (1986) *Ultrafiltration Handbook*; Technometric Publishing Company: Pennsylvania, USA.
46. Lapshin, R.V. (1995) Analytical model for the approximation of hysteresis loop and its application to the scanning tunneling microscope (PDF). *Review of Scientific Instruments* (USA: AIP) 66 (9): 4718–4730.
47. Love, A.E. (1927) *Treatise on the Mathematical Theory of Elasticity (Dover Books on Physics & Chemistry)*; Dover Publications: New York.
48. Mielke, A.; Roubicek, T. (2003) A rate-independent model for inelastic behavior of shape-memory alloys. *Multiscale Model. Simul.*, 1 (4): 571–597.
49. Sharma, R.R.; Chellam, S. (2005) Temperature effects on the morphology of porous thin film composite nanofiltration membranes. *Environ. Sci. Technol.*, 39 (13): 5022–5030.
50. McKeown, N.B.; Budd, P.M.; Book, D. (2007) Microporous polymers as potential hydrogen storage materials. *Macromol. Rapid Commun.*, 28: 995–1002.